UCRL-10515

University of California

Ernest O. Lawrence Radiation Laboratory

TWO-WEEK LOAN COPY

This is a Library Circulating Copy which may be borrowed for two weeks. For a personal retention copy, call Tech. Info. Division, Ext. 5545

YIELDING AND PLASTIC FLOW IN NIOBIUM

Berkeley, California

DISCLAIMER

This document was prepared as an account of work sponsored by the United States Government. While this document is believed to contain correct information, neither the United States Government nor any agency thereof, nor the Regents of the University of California, nor any of their employees, makes any warranty, express or implied, or assumes any legal responsibility for the accuracy, completeness, or usefulness of any information, apparatus, product, or process disclosed, or represents that its use would not infringe privately owned rights. Reference herein to any specific commercial product, process, or service by its trade name, trademark, manufacturer, or otherwise, does not necessarily constitute or imply its endorsement, recommendation, or favoring by the United States Government or any agency thereof, or the Regents of the University of California. The views and opinions of authors expressed herein do not necessarily state or reflect those of the United States Government or any agency thereof or the Regents of the University of California.

Submitted to Acta Metallurgica

UCRL-10515

UNIVERSITY OF CALIFORNIA
Lawrence Radiation Laboratory
Berkeley, California

Contract No. W-7405-eng-48

YIELDING AND PLASTIC FLOW IN NIOBIUM

L. I. Van Torne and G. Thomas

November 1962

YIELDING AND PLASTIC FLOW IN NIOBIUM

by

L. I. Van Torne and G. Thomas

Department of Mineral Technology and
Inorganic Materials Research Division
Lawrence Radiation Laboratory
University of California, Berkeley

ABSTRACT

A detailed comparison has been made of the substructures and mechanical properties of polycrystalline niobium deformed at room temperature. The results show that the lower yield stress depends upon the total impurity content, and that solute atom clusters are the strongest barriers to dislocation motion. It is concluded, however, that impurities are not responsible for the temperature dependence of the yield stress. The yield drop is shown to be due to dislocation multiplication and the effect of grain size on the yield and flow stress appears to be significant through the dislocation density. Dislocation cell structures are formed only in impure Nb containing dispersed precipitates. In the purest Nb dislocations are uniformly distributed, and this material exhibits very little work hardening. Work hardening is thus attributed to the long-range stress fields of cell walls or tangles. Dislocations were never observed to be extended and cross-slip is an easy process in Nb. This is consistent with Nb having an intermediate or high stacking fault energy.

1. INTRODUCTION

Whilst transmission electron microscopy has been widely utilized to correlate the microstructures and properties of FCC metals, not nearly as much attention has been paid to BCC systems, although iron has been investigated in some detail (e.g., see Keh[1]) and some work has been reported on Mo,[2] Ta,[3] and W.[4] So far, most of these investigations have been concerned with work hardening.

Yielding and plastic deformation in BCC materials are usually investigated in terms of the empirical Petch relationship initially established for ferrous materials.[5] This relationship is

$$\tau_y = \tau_f + K^* d^{-\frac{1}{2}}$$

where τ_y = yield stress, τ_f = friction stress, K^* is a parameter applying to the given metal (which is often taken as a measure of dislocation unlocking) and 2d is the average grain diameter. The research described here was done to try to understand in more detail the physical significance of the terms in the Petch relationship by a detailed comparison of substructures with mechanical properties. In this way, an attempt has been made to answer certain questions with regard to the plastic behavior of BCC metals, e.g., (1) What is the significance of the friction stress? (2) Is dislocation unlocking as important as has been thought and what causes discontinuous yielding and the yield drop? (3) What is the temperature dependent part of τ_y? and (4) What effect does grain size have on the yield and flow stress since the validity of using thermal-mechanical methods for changing grain size is open to question, for we have discovered that this may change

the composition and, if so, the Petch relationship is no longer obeyed. Furthermore, the grain size concept in terms of dislocation unlocking and pile-ups cannot be correct, since pile-ups are not observed in BCC metals,[6] nor does this explain the yield points of single crystals (e.g., see Hahn[7]).

2. EXPERIMENTAL PROCEDURE

2.1 Material Analysis

The Nb sheet used in this investigation was of the highest purity commercially available at the time. The chemical analysis of the as-received Nb is given in Table 1.

Table 1

Element	Group I (Kawecki Chem. Corp.)	Group II (Stauffer)
Al	<0.002	0.0165
C	0.002	<0.0020
Fe	0.010	0.0292
N_2	0.007	<0.0020
O_2	0.018	0.0288
Si	<0.010	0.0150
Ta	0.061	
Ti	<0.015	0.0060
H_2	0.001	

Chemical Analyses (Wt %) of As-received Nb Specimens

The specimens were reduced about ten percent by cold rolling prior to annealing. Annealing of the specimens in a vacuum of 10^{-6} to 10^{-5} mm Hg was employed to remove the interstitials, such as carbon, nitrogen, oxygen, and hydrogen. The efficiency of removal depends on the leak rate and best results were obtained with a one-liter capacity heat-treatment furnace.

Chemical analyses were always done on each specimen after each heat treatment. The analysis of the gases, namely nitrogen, oxygen, and hydrogen was done by a vacuum fusion technique, whilst the carbon content was determined by a conductometric method. The results are shown in Table 2.

2.2 Specimen Preparation

The material, 0.005 inches thick, was cut into tensile specimens three inches long by one-half inch wide, and was then annealed. The annealing temperatures and times employed were those yielding the best quality vacuum. The temperatures used did not exceed 2100°C and the time at temperature was never less than two hours. At the end of the anneal the furnace was cooled slowly, the time to come to ambient temperature being about two hours. By varying the annealing temperature it was possible to vary the impurity content of the initial Nb. This also resulted in different grain sizes. The measured grain size was taken as the arithmetical average of results obtained from five different areas of the specimen (Table 2).

The specimens were deformed at room temperature in an Instron Universal testing machine at a strain rate of 3.33×10^{-4} sec^{-1}. Thin foils, about 3000 Å thick, suitable for transmission electron microscopy were then prepared from the tensile deformed specimens using the "window technique" of chemical polishing. This enabled a direct comparison of microstructure and properties to be made. The polishing solution consisted of 40 vol. percent concentrated hydrofluoric acid and 60 vol. percent concentrated nitric acid. The temperature of the polishing solution was maintained just above 0°C by means of an ice bath. Satisfactory foils were obtained with this technique in about 30 minutes, whence they were examined in a Siemens Elmiskop 1b electron microscope operated at 100 kV.

2.3 Dislocation Density Measurements

The dislocation densities were determined by a technique described by Ham.[8] The relation for the dislocation density ρ is:

$$\rho = \frac{2N}{Lt} \quad \text{(valid for } N > 50\text{)}$$

where N = number of dislocation intersections with the random lines

L = total length of random line

t = foil thickness

The value used for the foil thickness, t, was determined from analyses of slip traces, using simple trigonometric relations. The value of t, so determined, was about 3000 Å. Since slip traces were infrequently observed, except in the purest specimens, it was not possible to determine the exact thickness for each of the many micrographs used for dislocation density determinations. Figure 1 shows an example of slip traces in a foil ~ 3000 Å thick.

The electron beam intensity in regions of the foils where dislocation density micrographs were taken was nearly equal to the intensity observed where t was determined from the slip trace. The tilting mechanism on the microscope was fully utilized to obtain the best contrast and maximum intensity in all foils under the same illumination conditions. Hence, only minimum error was introduced in using t equal to 3000 Å for all the micrographs.

Micrographs for density measurements were taken from five foils, each of which were taken from five different regions of the specimen gauge length. The area sampled by each micrograph is 15.75 square microns. The dislocation density was always observed to be less near the edges of the foils; therefore, all micrographs were taken as far from the foil edge as possible.

2.4 Other Data Obtainable from Electron Micrographs

The yield strength of a crystal containing a dispersion of internal stress centers is influenced by the scale of dispersion.[9] In a crystal these stress centers can be any obstacles which hinder dislocation motion, e.g., precipitate particles or clusters of solute atoms or vacancies. An example of the measurement of the distance between stress centers λ, i.e., the wavelength of a pinned dislocation between clusters (see section 3.1.3) is shown in Fig. 2(a).

An indication of the effect of friction on dislocation motion imposed by the crystal structure and solute atoms in solution can be obtained from observations of the radius of curvature of isolated dislocations. If it is assumed that in the absence of jogs or any applied stress the dislocation curvature is due to equilibrium between the line tension and the friction stress of the crystal, then the friction stress can be calculated from the measured radius of curvature. Examples of how this radius of curvature was measured are shown in Fig. 2(b). It is quite clear that many radii orientations are possible, but the true radius can be obtained by orthographic projection since the foil orientation can be determined by selected area diffraction. In order to make the assumptions more valid, only smoothly curving dislocations far from resolvable sources of internal stress were measured.

3. EXPERIMENTAL RESULTS

3.1 Tensile Stress-Strain Curves

Upon deformation, niobium exhibits a semidiscontinuous stress-strain tensile curve. A series of tensile stress-strain curves typical of more than 50 tests of polycrystalline Nb of various purity levels are shown

in Fig. 3. It is immediately evident that the level of impurity has a marked influence on the stress-strain curve and that this overrides the grain size effect (e.g., compare curves "D" and "E"). The purity for each group is given in Table 2. The effect of increasing the impurity content is to shift the portion of the curve in the plastic strain range to higher stress levels.

Table 2

Tensile Curve	Atom Fraction of Impurity (metallic + interstitial)	Grain Size (μ)
"A"	2.60×10^{-3}	490
"B"	3.80×10^{-3}	20
"C"	5.30×10^{-3}	177
"D"	6.50×10^{-3}	750
"E"	1.50×10^{-3}	700

Impurity Levels Corresponding to Tensile Curves Obtained from Specimens Groups A-E (Fig. 3)

Tensile curve "B" in Fig. 3 is conspicuous since this curve has a greater increase in flow stress for a given increment in strain when compared to the other curves. Tensile curve "B" represents a group of specimens that were used in the as-received, annealed condition. The annealing treatment reported for this group was 1000°C for two hours in a vacuum pressure of less than 10^{-5} mm Hg. Since the yield strength corresponds to Nb in the annealed condition for the given impurity level, the annealing cycle was accepted as reported. All the other specimens which are represented by the tensile curves "A", "C", "D" and "E" were annealed by us, as was discussed in the experimental procedure.

There was a very striking difference in the substructures of the specimens corresponding to tensile curve "B" as compared to the substructures in specimens which gave the other tensile curves. In "B" specimens there exist precipitate plates along dislocation networks, as shown in Fig. 4. This type of substructure is common to all the specimens giving curves of type "B"; however, it was not observed in the other specimens. This suggests that in the annealing range 1000-1300°C, niobium is not fully recrystallized and that the networks in Figure 4 correspond to a recovered condition.

It is generally accepted that the plastic deformation of BCC metals is concomitant with the initiation of a Lüders band at points of stress concentration within the specimen. Deformation then proceeds by the growth and lengthening of the band as it moves across the specimen. Nb plastically deforms in a similar manner. Lüders bands have been observed on the surfaces of deformed specimens, and an example is shown in Fig. 5. These bands originated at the junction of the specimen and the tensile grips. As the specimen deforms, the bands propagate across the specimen at an angle of about 45° to the tensile axis, which is, of course, the direction of the maximum shear stress. The band front progresses from the tensile grips toward the center of the gauge length.

3.1.2 Upper Yield Point

Upper yield points were observed for all the Nb specimens. If the specimen was unloaded after the upper yield point had appeared and then immediately reloaded, no upper yield point was observed upon subsequent reloading. The average magnitude of the yield drop was observed to be 0.40 $(\frac{kg}{mm^2})$.

3.1.3 Lower Yield Point

The lower yield stress is a more reproducible measure of the strength of the specimen since τ_{ly} is not as sensitive to specimen alignment in the tensile machine as τ_{uy}.* Therefore, the lower yield stress was considered to be a better measure of the strength of the specimen.

When τ_{ly} is plotted versus the atom fraction of metallic plus interstitial impurities (O, N, C, and H) a straight line of positive slope results, as shown in Fig. 6. The range of τ_{ly} observed is shown together with the average of the range. A least squares fit of the average points yields:

$$\tau_{ly} \left(\frac{kg}{mm^2}\right) = 1.75 + \left\{1.26 \times 10^3 \times (\text{atomic fraction})\right\} .$$

Impurities can affect the yield strength in a number of ways. They may be effective as solid-solution strengtheners or through clustering or precipitation. Precipitate plates large enough to obtain a selected area diffraction pattern have not yet been observed (Fig. 4). However, these plates are thought to be some form of niobium carbide. This is based on internal friction measurements of the carbon peak in Nb of comparable purity made by Powers and Doyle.[10] They found that the carbon peak decreased as the number of aging treatments increased. This suggests that the carbon is involved in the precipitation of some second phase or is clustering. Furthermore, similar appearing precipitate plates on dislocations have been observed by Keh and Leslie[11] in an aged Fe-Si-C alloy, and were identified as carbides.

The most obvious barrier to the motion of dislocations observed in specimens annealed at all the temperatures, including 1000°C, is the

---

*Throughout this paper τ refers to shear stress, which is taken as one-half the measure tensile stress σ.

presence of very small, nearly spherical "clusters," the contrast from which is sensitive to specimen orientation (Fig. 7). This suggests that each cluster has with it an associated strain field, e.g., similar to a dislocation loop. These barriers together with dislocations interacting with them can be seen in Fig. 7(c). Further, clusters associated with dislocations can be resolved by tilting dislocations out of contrast. The measured diameter of these particles ranges from 50 to 150 Å, and their volume fraction increases with % interstitials. A bright field image of a (112) foil together with a ($\bar{1}10$) dark field image of the same area is shown in Figs. 7(a) and (b). It can be observed that the contrast from some of these specks arises from the ($\bar{1}10$) reflection. Note the bright spots in the dark field image that correspond to dark spots in the bright field image. Hence, it is thought that the contrast arises from clusters of solute atoms. The contrast does not arise solely from dislocation loops or dislocations perpendicular to the foil surface. These particles can be observed, e.g., Fig. 7(d), in fully annealed undeformed specimens. Clearly, there are no dislocation loops associated with them. In Fig. 7(a) the contrast is greatest on one end of the elongated loop, indicating that the loop is pinned on one side. In Fig. 7(b) the maximum brightness in dark field corresponds to the pinned side of the loop and the pinned end of the dislocation line. Such observations indicate that the clusters are making the maximum contribution to the contrast.

Nabarro[12] has considered the hardening effect of long-range stress fields of isolated atoms or clusters in polycrystals. In his analysis the yield stress is given approximately by:

$$\tau = G\epsilon^2 c$$

where G = shear modulus, for Nb, $G = 3.82 \times 10^3 \left(\frac{kg}{mm^2}\right)$ (13)

ϵ = an atomic misfit parameter defined by:

$$\epsilon = \frac{(r_{solute} - r_{solvent})}{r_{solvent}}$$

r_{solute} = radius of the solute atom
$r_{solvent}$ = radius of the solvent atom
c = the atom fraction concentration of solutes.

The values of r_{solute} used for the calculation of ϵ are shown in Table 3.

Table 3

Element	Atomic "Radius" (Å)	Ref.	$\epsilon = \frac{(r_{solute} - r_{solvent})}{r_{solvent}}$
Nb	1.429	(14)	o
Ta	1.430	"	0.670×10^{-3}
Ti(BCC)	1.45	"	1.47×10^{-2}
Si(DC)	1.18	"	-1.74×10^{-1}
Fe(BCC)	1.24	"	-1.32×10^{-1}
Al	1.43	"	0.670×10^{-3}
C	0.74	(15)	-4.82×10^{-1}
N	0.73	"	-4.89×10^{-1}
O	0.73	"	-4.89×10^{-1}
H	0.35	"	-0.755

Calculated Values for Atomic Radii
and Misfit Parameters for Solute Atom Impurities in Nb

When τ, calculated from the above expression, is plotted versus atomic fraction of impurity, the lower line in Fig. 6 is obtained. A linear least squares fit of a line to these points yields,

$$\tau \left(\frac{kg}{mm^2}\right) = \left\{1.09 \times 10^3 \left(\frac{kg}{mm^2}\right) \times c \text{ (atomic fraction)}\right\} - 0.705.$$

It is evident from this result that a theoretical model based on interactions of dislocation strain fields with the dilatational strain fields of solute atoms and/or clusters predicts a dependence of yield strength similar to what is observed. Such interactions do not contribute to the temperature dependence of τ_y except through the temperature dependence of G.

3.1.4 Friction Stress

The calculated values of τ_f from the measured radii r of isolated curved dislocations (Fig. 2(a)) are plotted versus atom fraction of impurities in Fig. 8. The dislocation curvature is assumed to be due to the atomic lattice-dislocation, solute atom-dislocation interaction or dislocation jogs that are not resolved. Since the solute atoms interacting with the dislocation are dispersed below the limit of resolution of the electron microscope, they are therefore considered to be in solution. The friction stress was calculated from the relationship:

$$\tau_f = \frac{Gb}{r}$$

where $r = (\frac{4}{\pi})r_p$ = radius of curvature

r_p = projected radius on the micrograph

$(\frac{4}{\pi})$ = a factor applied when assuming r_p to be randomly oriented.

The mean and τ_f plus and minus a standard deviation are shown. Each range represents not less than 19 measurements, nor more than 46. A least squares line for the mean points gives:

$$\tau_f \left(\frac{kg}{mm^2}\right) = 0.805 + \left\{0.279 \times 10^3 \times (\text{atom fraction})\right\}$$

The resulting line shows that τ_f depends on the impurity content of the crystal.

3.1.5 Flow Stress versus Plastic Strain

The relationship between the flow stress σ_f and plastic strain was determined for the two types of experimental tensile stress-strain curves. The values of σ_f and ϵ_p were taken from the tensile curve "B". A logarithmic plot of σ_f and ϵ_p yields the following relationship:

$$\sigma_f = \epsilon_p^{\frac{1}{4}} + \text{constant.}$$

Similarly, for the tensile curves of type "A", "C", "D" and "E", which are obviously different from type "B", σ_f and ϵ_p are related as follows:

$$\sigma_f = \epsilon_p^{\frac{1}{10}} + \text{constant.}$$

3.2 Dislocation Density

In order to determine the relationship between the dislocation density, flow stress, and plastic strain, the same log-log method used for the relations between observed stress and strain was employed. The relationship between dislocation density and flow stress for specimens showing tensile curve type "B" is:

$$\sigma_f \left(\frac{kg}{cm^2}\right) = 0.85\ Gb\rho^{\frac{1}{2}} + \text{constant.}$$

The corresponding relation between plastic strain and dislocation density is:

$$\epsilon_p(\%) = 5.3 \times 10^{-20}\ \rho^2 + \text{constant.}$$

The values of the coefficients were determined by a linear least squares analysis of the average points of $\rho^{\frac{1}{2}}$ versus σ_f and ρ^2 versus ϵ_p, as shown in Figs. 9 and 10. The total range of ρ and the average of the range are shown.

It has been shown above that the flow stress σ_f for tensile curve "B" can be expressed in terms of the dislocation density by the relation:

$$\sigma_f = A\rho^{\frac{1}{2}} + \text{constant}$$

where A is a constant for a given condition. The plastic strain for this type tensile curve can also be expressed in terms of the dislocation density by the relation:

$$\epsilon_p = B\rho^2 + \text{constant}$$

where B is a constant.

Clearly, from these two relations obtained from dislocation density measurements, a relation between σ_f and ϵ_p can be obtained. The two above expressions give:

$$\sigma_f = C\epsilon_p^{\frac{1}{4}}$$

where C is a constant.

This is the same functional relation between σ_f and ϵ_p obtained from the experimental tensile curve. Hence, the relations between σ_f and ϵ_p obtained from dislocation density measurements, correlate with the relation between σ_f and ϵ_p obtained from the experimental tensile curve "B".

Since the observed flow stress-plastic strain relations are very different for the two types of tensile curves, the relation between flow stress and plastic strain with dislocation density would likewise be expected to be different. By applying the same log-log methods as above, the relation between flow stress and dislocation density for specimens showing tensile curves "A", "C", "D", "E" (now referred to as group A) was found to be:

$$\sigma_f \left(\frac{kg}{cm^2}\right) = 6.5 \times 10^3 \, Gb\rho^{\frac{1}{7}} + \text{constant}.$$

The relation between plastic strain and density is:

$$\epsilon_p(\%) = 2.52 \times 10^{11} \, \rho^{\frac{1}{7}} + \text{constant}.$$

The values of the coefficients were determined by a linear least squares analysis of $\rho^{\frac{1}{7}}$ versus σ_f and $\rho^{\frac{10}{7}}$ versus ϵ_p, as shown in Figs. 11 and 12. The total range of ρ and the average of the range are shown.

The range of ρ is larger at lower σ_f due to inhomogeneous deformation at this stress level. The bottom of the range represents ρ in front of the Lüders band front and the top of the range represents ρ behind the Lüders band front.

The observed stress-strain relation for tensile curve type "C" can also be derived from dislocation density versus flow stress and versus plastic strain relations. The result is

$$\sigma_f = C\epsilon_p^{\frac{1}{10}}$$

where C is a constant.

Hence, there is excellent correlation with dislocation density and the observed flow stress-strain relation for tensile curves of group A specimens.

3.3 Microstructural Changes with Deformation

The tensile behavior of specimens of group B is different from that of Group A. The dislocation substructures are also different. As was pointed out earlier, specimens B always contained precipitate particles on the grown-in dislocations, yet the amount of yield drop was no greater than in specimens of group A. During plastic deformation the dislocation density in the regions containing precipitates always increased rapidly with considerable tangling, leading eventually to the formation of well-defined cell boundaries (Figs. 13(a)-(c)). On the basis of current work-hardening theories, this behavior would predict that $\sigma_f \propto \rho^{\frac{1}{2}}$, as was found (Fig. 9). However, in specimens of group A, cell structures were never observed. Instead, dislocations were randomly distributed (Fig. 14(a)-(c)). For the same strain as specimen B the dislocation density was lower, and σ_f was found to be proportional to $\rho^{\frac{1}{7}}$ (Fig. 11). i.e., dislocations are relatively weak barriers in "pure" niobium. These results show that in order for

rapid multiplication and tangling of dislocations to occur, strong barriers, such as precipitate particles, must be present.

We do not attach any particular physical significance to the $\rho^{\frac{1}{7}}$ factor, e.g., it has been reported[16] that the work-hardening coefficient in Nb' varies with annealing treatment and therefore purity. What these results show is simply that the purer the material the smaller is the dependence of σ_f on dislocation density.

3.4 Effect of Grain Size on Yield Strength

Various grain sizes were obtained by the annealing cycles employed. As shown in Fig. 15, no discernable relation was observed between grain size and τ_{1y}, and the Petch law was not obeyed. However, the plot of τ_{1y} versus impurity content, also shown in Fig. 15, gave a linear relation of positive slope. Figure 3 shows that τ_{1y} is influenced more by the impurity content than by grain size. In turn, we have shown that the dislocation substructure is very dependent on the impurity content and annealing history of the specimen. Hence, if the impurity content changes from one grain size to another, the effect of grain size on τ_{1y} may be masked by changes in the dislocation substructure concomitant with changes in impurity level. It should be pointed out, therefore, that the method of varying grain size by annealing treatments in Nb should be done with the utmost caution since it is extremely difficult to anneal Nb without changing the impurity content and/or the manner in which it appears within the specimen.

4. DISCUSSION

4.1 Microstrain and the Yield Drop

This is the plastic deformation that occurs at strains below the upper yield. Originally[17] it was thought that microstrain occurred when dislocations became unlocked, moved and then started new sources when the pile-up stress was sufficiently large. There is no evidence for pile-ups in Nb (e.g., notice the profuse cross-slip in Fig. 1) and our results show that the main dislocation sources are at grain boundaries (e.g., Fig. 16) and precipitates (Fig. 13(a)). In an ideal single crystal the surface is probably the most effective source. Thus, these experimental results do not agree with the Cottrell-Bilby[18] hypothesis.

It has been suggested more recently[7, 18] that the microstrain and upper yield point depends on the number and velocity of mobile dislocations (which could be generated during the act of gripping the specimen in the tensile machine) and that the yield drop is associated with dislocation multiplication.

Dislocation density measurements at σ_{uy} and just approaching σ_{ly}, P to Q in Fig. 3, showed that a high rate of dislocation multiplication does occur in this portion of the stress-strain curve. In areas of the specimens where dislocation motion had occurred, the average dislocation densities (50 measurements) determined from five foils at P and five foils at Q (Fig. 3) from random regions of the specimens were:

at P, 8.6×10^8 (lines/cm^2) (Fig. 17(a))

at Q, 29.8×10^8 (lines/cm^2) (Fig. 17(b))

Thus $\Delta\rho = 21.2 \times 10^8$ (lines/cm^2)

This is an increase in dislocation density by a factor of about four. For an equivalent increment in strain over the work-hardening range, i.e., an amount equal to $\epsilon(Q) - \epsilon(P)$, the change in dislocation density was found to be 4.6×10^8 (lines/cm^2). Therefore, the dislocation multiplication rate is greater near the yield point than beyond σ_{ly}.

The mechanism of multiplication in the absence of precipitate barriers probably occurs by a double cross-slip process described for the BCC metals by Low and Guard[19] and Conrad.[20] Such cross-slip could occur at jogs, tangles or at subboundaries. Possible evidence for multiplication can be seen in Fig. 14(c), where the dislocation density is larger near loops than elsewhere. More obvious cases of multiplication can be seen around the precipitate particles and clusters in Figs. 13(b) and 7(c). Multiplication here can also take place by cross-slip, as suggested by Hirsch.[21] Any effective barrier to dislocation motion can thus be effective as a multiplication center. Thus, impurities seem to play an important role in increasing the dislocation density during plastic deformation.

These results demonstrate that it is unnecessary to invoke a process of dislocation unlocking to explain the yield drop. Conversely, it is the strong locking effect of barriers, such as precipitates, which provide the necessary sources for multiplication.

4.2 The Lower Yield Stress

Yielding of a crystal is influenced by the ease with which dislocations can move through it. The motion of a dislocation is influenced by any barrier that may lie in its path. Here, the shear stress required to

move dislocations through a crystal containing such barriers will be denoted by $\tau_{structure}$. Structure refers to anything excluding lattice friction that impedes the motion of the dislocations. Hence, the lower yield stress can be expressed by:

$$\tau_{ly} = \tau_{friction} + \tau_{structure}.$$

A plot of τ_f versus atom fraction of impurities appears in Fig. 8. The mean points and the limits of each range were determined by making a probability plot for the measured values of τ_f corresponding to a given purity level. These give the ranges I, II, III, IV and V in Fig. 8. The least squares line through the mean points of τ_f has a slight positive slope. Such a result shows that τ_f has some dependence on the amount of impurity atoms in solution. It should be made clear that the term "in solution" here means those solute atoms which are not clustered or in a precipitate phase large enough to be resolved in the microscope. Since τ_f shows some dependence on impurity content, it seems reasonable to factor τ_f into two terms, given by:

$$\tau_f = \tau_o + \tau_{soln.}$$

where τ_o = lattice friction of a pure crystal

$\tau_{soln.}$ = the friction contribution due to impurities in solution

If it is assumed that a linear relation between τ_f and atom fraction of impurities is valid for impurity levels approaching zero, an extrapolation of the line to zero impurities will give an estimate of τ_o. Such an extrapolation gives a value of τ_o of about 0.8 $(\frac{kg}{mm^2})$. This would be a maximum value since the curve of the mean points shows a tendency to non-linearity at the lower impurity levels.

The contribution of $\tau_{structure}$ to τ_{ly} is relatively large compared to τ_f. $\tau_{structure}$ is the contribution due to barriers in the crystal that impede the motion of dislocations.

The calculated values of $\tau_{structure}$ obtained for the various levels of impurities from the Nabarro analysis described in section 3.1.3 are shown in the lower curve of Fig. 6. A least squares line has been drawn for these points. The slope of the $\tau_{structure}$ line is nearly parallel to the observed τ_{ly} line, which is encouraging. However, $\tau_{structure}$ obtained from the expression

$$\tau_{st} = G\,\epsilon^2\,c$$

should pass through the origin when c is equal to zero. Possible reasons why the line does not pass through the origin are experimental errors in the determination of G and c as well as assumptions inherent in atomic radii in the calculation of ϵ. Since there is a constant difference in the line, the error is most probably in the chemical analysis from which c is obtained.

If the values of τ_f from Fig. 7 are added to τ_{st} the dashed line in Fig. 6 is obtained. The significance of the dashed line is that the slope is in excellent agreement with the slope of observed τ_{ly}. The constant difference in the two lines can be removed by shifting the $\tau_{structure}$ line so that it passes through the origin as it should at c equal to zero. On the other hand, the observed τ_{ly} line was obtained at a fixed strain rate and changes in strain rate will raise and lower the yield point. For example, the specimens whose average τ_{ly} is marked by a pyramid in Fig. 6 were strained at a strain rate one tenth less than the specimens in the range immediately above. Notice that τ_{ly} for $\frac{\dot{\epsilon}}{10}$ cluster on the dashed line. The

effect of an increase in strain rate is to magnify the stress-strain curve.[18] Since the observed τ_{ly} line is parallel to τ_{ly} calculated from τ_f and $\tau_{structure}$, the yield strength of niobium is determined primarily by the total impurity content.

Mordike and Haasen[22] have recently proposed that dislocation-precipitate interactions are the most likely cause of the thermal contribution to the yield stress. However, this is true only if dislocations can cut through obstacles (e.g., see Kelly[23]). The stress necessary to accomplish this process is given[23] at 0°K, by

$$\tau_c = \frac{\pi}{2} \frac{\gamma r}{\lambda b}$$

where γ is the energy of the interface produced when the particle is sheared, r is the particle radius, and λ is the interparticle spacing in the path of the dislocation. The maximum work done during cutting is the initial shearing of bonds in the cluster. γ may be estimated from the above equation for the size and spacing of the observed clusters. τ_c at 0°K is ~ 50 kg/mm^2 (this value is obtained by extrapolating the τ_y vs T curve obtained from ref. 24) and for r ~ 50 Å, λ ~ 500 Å (Fig. 2(a)), γ is ~ 0.14 eV/atom bond, which is rather large. It is difficult to estimate the bond strength in the cluster when the species are unknown. The most likely solute atoms in the cluster appear to be carbon[10] or nitrogen (Wert, private comm.). Table 4 shows some estimated values of bond strengths for a few possible cluster species.

The maximum size of cluster r which permits cutting is[23]

$$r = 2Gb^2/\pi\gamma.$$

From Table 4, for the weakest cluster, i.e., oxygen atoms, r_{max} is only 10 Å. For carbon, nitrogen or mixed species in the cluster, r_{max} is less

Table 4

Bond	C-C*	N-N*	O-O*	Nb_2N^+	NbN^+	NbC^+	$Nb_2O_5{}^+$	$Nb_2O_4{}^+$
Energy eV per interstitial atom (298°K)	1.8	0.83	0.73	2.7	2.5	1.3	4	4

Data calculated from: *Pauling, Nature of the Chemical Bond, Cornell University Press, 1960.

†Miller, Metallurgy of Niobium and Tantalum, Butterworths, 1959.

Estimated Bond Energies for Possible Cluster Species in Nb.

than 10 Å. Thus, in general, cutting of clusters by dislocations is an unlikely process, so that clusters do not appear to be responsible for the temperature dependence of the yield stress. Furthermore, impurities in solution only affect τ_f and $\tau_{structure}$ athermally; hence, the only temperature dependent part of τ_y must be τ_o. τ_o can thus be associated with the Peierls-Nabarro stress since this is now thought to be the most important thermal component of τ_y.[25]

4.3 Flow Stress

It was shown in section 3.3 that the differences in tensile behavior between groups A and B are related to the differences in substructures. The formation of well-defined cell structures in group B are similar to those observed in other BCC and also FCC metals of intermediate stacking fault energies. The boundaries of the cells are composed of very dense regions of dislocations surrounding relatively dislocation-free areas, e.g., Fig. 13(c). In specimens of group A the dislocations are arranged randomly but produce many tilts within a grain, as shown by the changes in

contrast (Fig. 14(b)). It should be noticed that these tilts lie within areas of dislocation cross-over. Washburn[26] has shown that cross-over may be an important mechanism for multiplication. In Fig. 13 the cell structure has developed from dislocation tangles formed at the precipitate plates existing on the original dislocations. There were no dislocation cell boundaries observed in the specimens represented by the substructure shown in Fig. 14. Furthermore, specimens showing a tensile curve of type "C" have been deformed to about 22 percent elongation without observing any dislocation cell structure formation. No evidence was obtained for the formation of lengths of <100> dislocations in fully annealed Nb as has been observed in Fe,[1, 6] Mo[2] and Ta.[3]

It is likely that much more severe deformation is required to develop a cell structure in Nb when the specimen is deformed at room temperature. However, Keh and Weissmann[6] have observed a temperature dependence of the onset of cell formation in Fe. The tendency for cell formation is retarded as the temperature at which deformation occurs is lowered. This is thought to be due to the higher frictional stress at lower temperatures. It is also clear from our results that whether or not cells form depends upon the impurity level and on how the impurities are dispersed. Thus, depending on purity in Nb, and in view of the higher melting point of Nb than Fe, a cell structure may not be observed for any deformation at ambient temperature.

The current theories of work hardening in metals[27-30] predict a flow stress that is a linear function of the square root of the dislocation density. These theories are based on cell structure formation or some type of well-defined regions of high dislocation density. It has been shown that a well-defined cell structure only develops with tensile deformation

in the specimens containing networks of precipitates which result in a tensile curve of type "B". Further, the flow stress for these specimens is a function of the square root of the dislocation density.

Specimens which give tensile curves of group A do not form cell structures; neither do they work harden very much (Fig. 3). One concludes therefore, that cell formation is one of the most important causes of work hardening in Nb. In both groups of specimens many dislocation loops and dipoles are observed (Figs. 13, 14). These may be formed from heavily jogged dislocations or intersections in a variety of ways. Since specimens of group B work harden faster than those of group A, loops and dipoles themselves cannot be very strong barriers to dislocation motion, although they probably play an important role in multiplication. These facts would give support to Li's theory[30] that work hardening arises from the long-range stresses due to tangles and cell walls and would explain the differences in work-hardening rates in the two groups of specimens.

4.4 Significance of Grain Size on σ_f

Figure 18 shows the dislocation density vs σ_f for two samples of Nb of corresponding purity but with the grain size in X being ~ 10 times that in Y. These results, together with those of Figs. 9-12, show that if σ_f is controlled by the dislocation density, the same value of σ_f for a single crystal and a polycrystal would only be arrived at after very large differences in strain. This suggests that changes in grain size really signify changes in dislocation density. For example, for specimens exhibiting cell structures, as shown in Fig. 9, $\sigma_f = \sigma_o + mGb\rho^{\frac{1}{2}}$. If this is equated to the Petch relationship, it is easy to show that $\rho \propto \frac{1}{d}$. The actual variation of ρ with d will depend on how σ_f varies with ρ. This may explain why a σ_f

vs grain size plot often fits various functions of d. This result is most easily explained if grain boundaries are the important sources for dislocations. Ample evidence for this has been obtained in these experiments (e.g., see Fig. 16) and other workers have also observed grain boundary sources in many materials. In an ideal single crystal the only "boundary" sources would be at the free surfaces and these could be introduced during handling. In the simplest model the maximum free path of travel of a dislocation before interaction with another would be about half the grain diameter. In polycrystals, therefore, the finer the grain size, the greater the number of sources and the shorter the interaction distance. Thus, all other things being equal, σ_f will increase with decreasing grain size, as is observed experimentally. It appears, therefore, that the parameter K^* in the Hall-Petch equation is associated with the dislocation density and may be related to the stress required to operate grain boundary sources, as suggested earlier by Conrad and Schoeck.[31]

5. SUMMARY AND CONCLUSIONS

1. The lower yield stress of impure polycrystalline Nb can be expressed by

$$\tau_{ly} = \tau_f + \tau_{structure} + \tau(\dot{\varepsilon})$$

where τ_f = friction stress = $(\tau_o + \tau_{soln.})$

$\tau_o \doteq 0.8 \left(\frac{kg}{mm^2}\right)$ (lattice friction stress)

$\tau_{soln.} = 0.279 \times 10^3 \times$ (atom fraction of impurities)
(friction stress due to impurities atomistically in solution)

$\tau_{structure}$ = stress due to (i) dilatations in the crystal from solute atom clusters and precipitates and (ii) dislocation-cluster interactions.

$\tau(\dot{\varepsilon})$ = strain rate dependence of the yield strength.

The only thermal contribution to τ_{ly} appears to be through τ_o.

2. The results show that dislocation unlocking is an unnecessary concept to explain the yield drop. Direct evidence has been given to show that the yield drop is accompanied by a large and rapid increase in dislocation density by multiplication, probably through cross-slip. Cross-slip is observed to be an easy process in Nb.

3. The strongest barriers to dislocations for the purities investigated appear to be solute atom clusters.

4. The flow stress-plastic strain relation determined from dislocation density measurements correlates with the experimentally observed flow stress-plastic strain relation.

5. The flow stress of polycrystalline Nb is markedly influenced by the initial dislocation substructure. The presence of precipitate net-works gives rise to cell formation on plastic deformation producing a flow stress-dislocation density dependence of

$$\sigma_f \left(\frac{kg}{cm^2}\right) = 0.85\ Gb\rho^{\frac{1}{2}} + \text{constant.}$$

The flow stress-dislocation density dependence in fully annealed polycrystalline Nb where cells are not observed is given by

$$\sigma_f \left(\frac{kg}{cm^2}\right) = 6.5 \times 10^3\ Gb\rho^{\frac{1}{7}} + \text{constant.}$$

Thus, the tendency for cell structure formation depends strongly on impurities. Neither stacking faults nor dislocation pile-ups were observed in this work.

6. The grain size dependence of σ_y and σ_f has been shown to be significant through the dislocation density.

7. From these conclusions, it is possible to predict the lower yield point and flow stress for polycrystalline Nb when the impurity level and annealing conditions are known.

ACKNOWLEDGMENTS

This research was done in partial fulfillment for the M.S. degree in the University of California (L.I.V.T.). The authors are grateful to the United States Atomic Energy Commission for financial support of this work.

REFERENCES

1. A. S. Keh, Direct Observations of Imperfections in Crystals, Eds., Newkirk and Wernick, p. 213, Interscience, New York (1962).

2. R. Benson, G. Thomas and J. Washburn, Direct Observations of Imperfections in Crystals, Eds., Newkirk and Wernick, p. 375, Interscience, New York (1962).

3. D. Hull, Electron Microscopy and Strength of Crystals, Eds., Thomas and Washburn, p. 291, Interscience, New York (1962).

4. Y. Nakayama, S. Weissmann and T. Imura, Direct Observations of Imperfections in Crystals, Eds., Newkirk and Wernick, p. 573 Interscience, New York (1962).

5. E. O. Hall, Proc. Phys. Soc. B64, 747 (1951); N. J. Petch, J. Iron and Steel Institute, 174, 25 (1953).

6. A. S. Keh and S. Weissmann, Electron Microscopy and Strength of Crystals, Eds., Thomas and Washburn, p. 231, Interscience (1962).

7. G. T. Hahn, Acta Met. 10, 727 (1962).

8. R. K. Ham, Phil. Mag., 6, 1183 (1961).

9. A. H. Cottrell, Dislocations and Plastic Flow in Crystals, Oxford Clarendon Press (1953).

10. R. W. Powers and M. V. Doyle, J. of Metals, 1285, New York (1957).

11. A. S. Keh and W. C. Leslie, "Recent Observations on Quench-Aging and Strain-Aging of Iron and Steel," North Carolina State College Conference (March 1962) to be published by Interscience Publishers.

12. F. R. N. Nabarro, Proc. Phys. Soc. 58, 669 (1946).

13. M. B. Reynolds, Trans. A.S.M., 45, 396 (1953).

14. C. S. Barrett, Structure of Metals, 646-648, McGraw-Hill, New York (1952)

15. W. Hume-Rothery and G. V. Raynor, The Structure of Metals and Alloys, p. 66, Inst. of Metals, London (1956).

16. Pratt-Whitney Aircraft Co. Report #375 (1962).

17. A. H. Cottrell and B. A. Bilby, Proc. Phys. Soc. A62, 49 (1949).

18. W. G. Johnston, J. Appl. Phys. 33, 2716 (1962).

19. J. R. Low and R. W. Guard, Acta Met. 7, 171 (1959).

20. H. Conrad, J. Iron, Steel Inst. (London) 198, 364 (1961).

21. P. B. Hirsch, Appendix to G. Thomas and J. Nutting, J. Inst. Metals 86, 13 (1957).

22. B. L. Mordike and P. Haasen, Phil. Mag., 7, 459 (1962).

23. A. Kelly, Electron Microscopy and Strength of Crystals, Eds., Thomas and Washburn, p. 947, Interscience, New York (1962).

24. M. A. Adams, A. C. Roberts and R. E. Smallman, Acta Met., 8, 328 (1960).

25. H. Conrad, Conference on Structure and Properties (N.P.L. England) 1963, to be published.

26. J. Washburn, Strengthening Mechanisms in Solids, p. 51, A.S.M. (1962).

27. A. Seeger, Dislocations and Mechanical Properties of Crystals, p. 243, John Wiley & Sons, New York (1957).

28. G. Saada, Acta Met. 3, 200 (1960); Acta Met. 8, 341 (1960); Acta Met. 9, 166 (1961).

29. P. B. Hirsch, Phil. Mag. 7, 67 (1962).

30. J. C. M. Li, Discussion of paper by Keh, Direct Observations of Imperfections in Crystals, Eds., Newkirk, Wernick, p. 234, Interscience, New York (1962).

31. H. Conrad and G. Schoeck, Acta Met. 8, 791 (1960).

Table Captions

1. Chemical Analyses (Wt %) of As-received Nb specimens.

2. Impurity Levels Corresponding to Tensile Curves Obtained from Specimens Groups A-E (Fig. 3).

3. Calculated Values for Atomic Radii and Misfit Parameters for Solute Atom Impurities in Nb.

4. Estimated Bond Energies for Possible Cluster Species in Nb.

Figure Captions

1. Showing cross-slip in a Nb thin foil ~ 3000 Å thick. The dislocation A is almost pure screw. The traces B correspond to slip and cross-slip on $(01\bar{1})$ and (110). Orientation [010].

2(a). Showing pinning distance λ between clusters.

(b). Showing curved dislocations of projected radius r_p from which friction stress is determined.

3. Typical tensile stress-strain curves for Nb of the various impurities investigated.

4. Nb containing 3.8×10^{-3} at fraction total impurities after recovery anneal at 1000°C, showing platelets of precipitate along dislocation networks.

5. Lüders bands on foil surface of tensile deformed Nb.

6. Plot of τ_{ly} and τ calculated for impurity strain fields versus atom fraction total interstitial impurities.

7. Observations of solute atom clusters in Nb (a) bright field image of [112] foil (b) corresponding $(\bar{1}10)$ dark field image (c) interaction between dislocations and clusters (notice loops at A) (d) clusters in as-annealed condition. Nb purity = 4×10^{-3} total atom fraction.

8. Plot of τ_f vs atom fraction total impurities in Nb.

9. Plot of square root of dislocation density vs flow stress for group B specimens.

10. Plot of square of dislocation density vs % plastic strain for group B specimens.

11. Plot of seventh root of dislocation density vs flow stress for group A specimens.

12. Plot of $\rho^{(10/7)}$ vs % plastic strain for group A specimens.

13. Change in dislocation substructure with strain for group B specimens deformed at room temperature (a) 1% strain (b) 5% strain (c) 12% strain. Notice tangling and multiplication near precipitates and cell formation in (c).

14. Change in dislocation substructure with strain for group A specimens (a) 2% strain (b) 5% strain (c) 12% strain. Notice smaller change in ρ with strain compared to Fig. 13 and multiplication near loops A.

15. Plot of lower shear yield stress vs % total atom fraction impurity and grain size.

16. Grain boundary sources in Nb.

17(a). Typical dislocation density corresponding to point P, Fig. 3.
(b). Typical dislocation density corresponding to point Q, Fig. 3.

18. Plot of dislocation density vs flow stress for two different grain sizes but same impurity level (4×10^{-3} atom fraction).

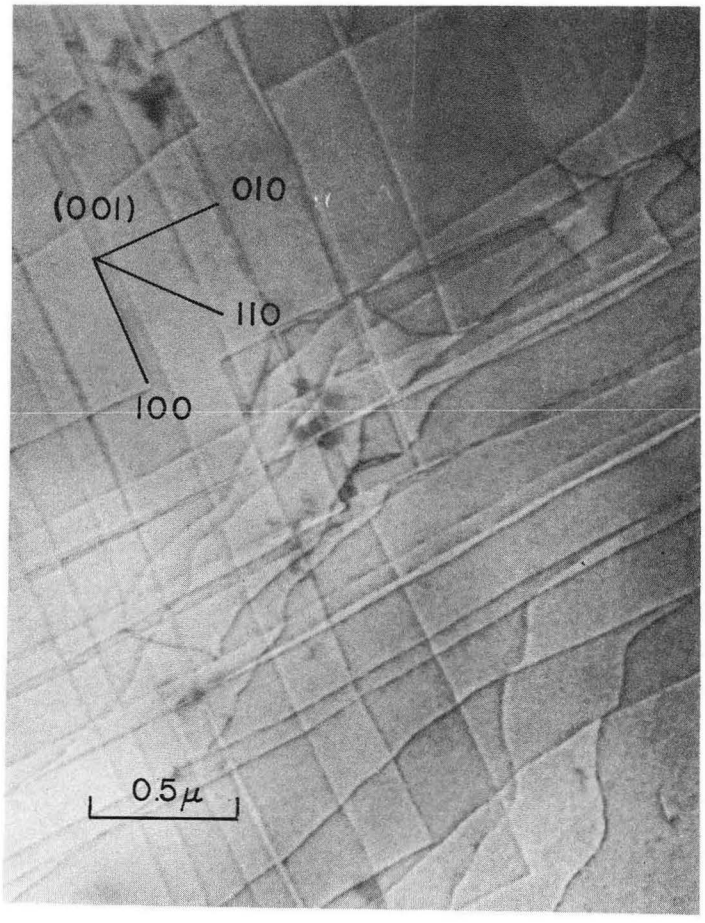

ZN-3465

Fig. 1.

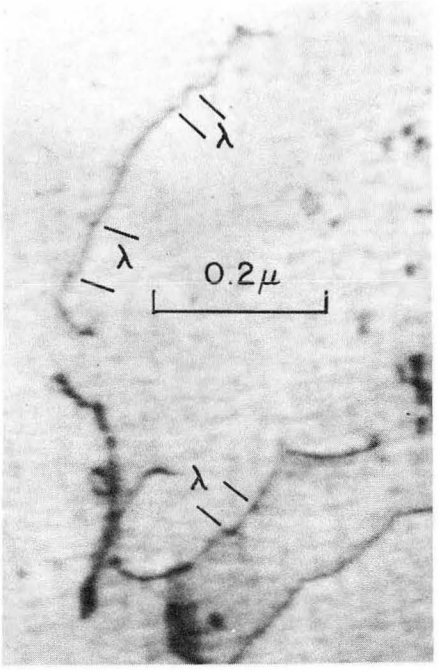

ZN-3466

Fig. 2(a).

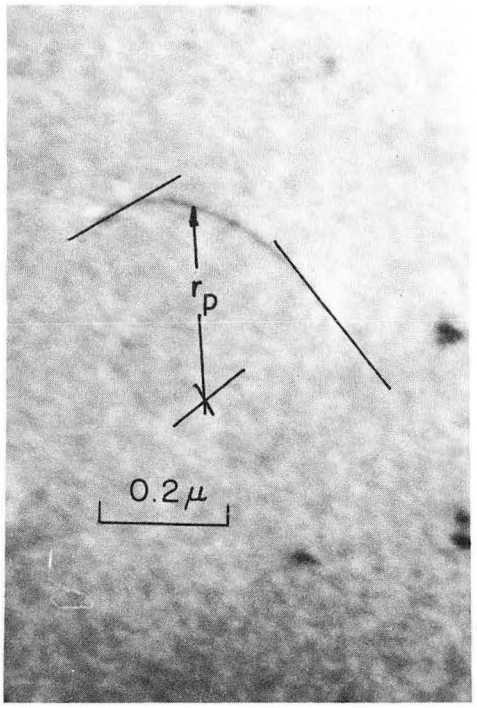

ZN-3467

Fig. 2(b).

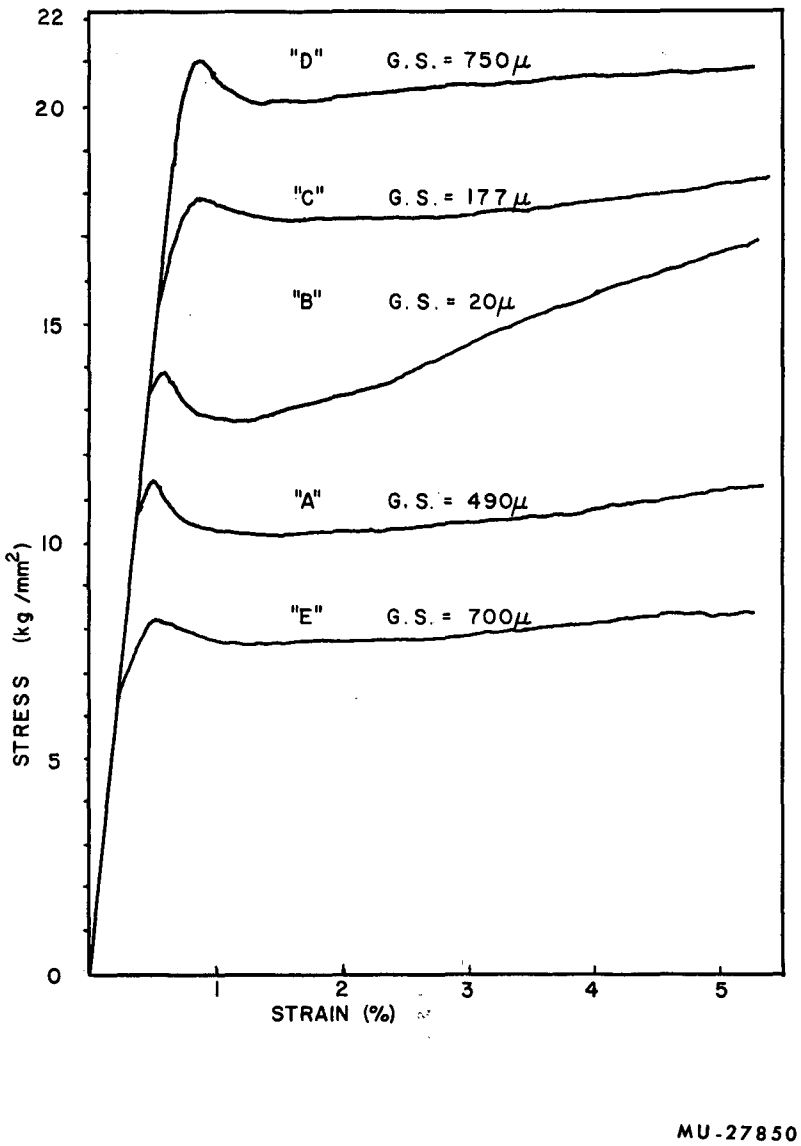
22
20
15
10
5
0
STRESS (kg /mm²)
"D" G.S. = 750μ
"C" G.S. = 177μ
"B" G.S. = 20μ
"A" G.S. = 490μ
"E" G.S. = 700μ
1
2
3
4
5
STRAIN (%)
MU-27850

Fig. 3.

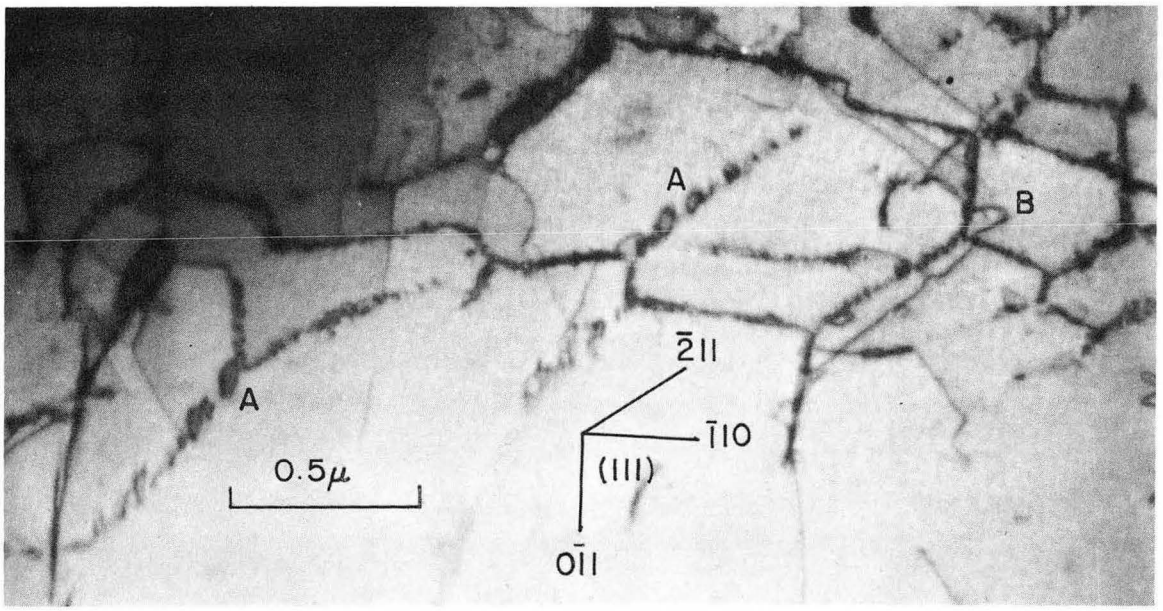

ZN-3460

Fig. 4.

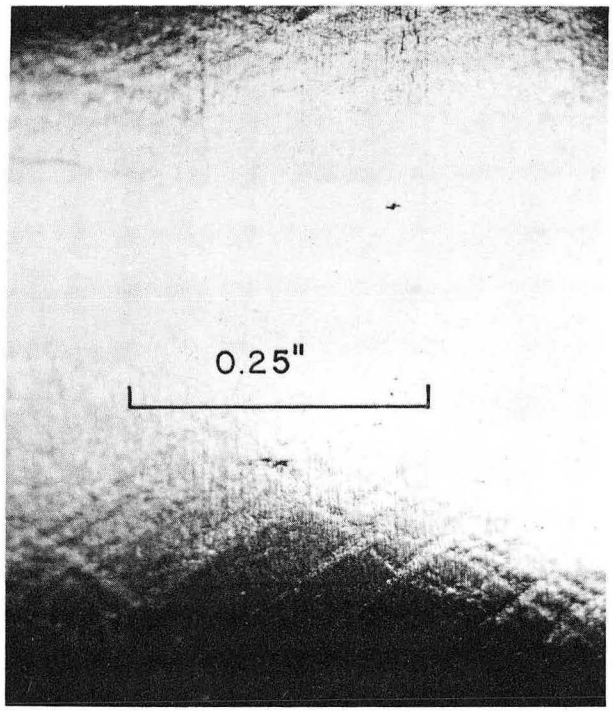

ZN-3461

Fig. 5.

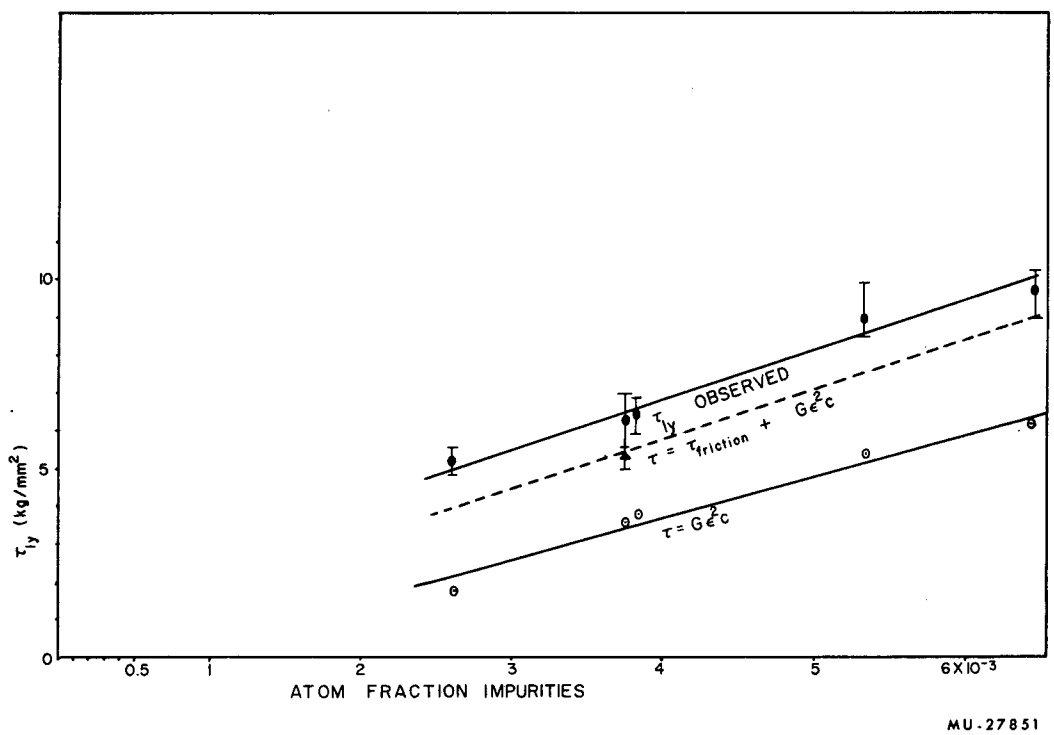
10
5
0
τ_{ly} (kg/mm^2)
0.5
1
2
3
4
5
6X10^{-3}
ATOM FRACTION IMPURITIES
OBSERVED
τ_{ly}
$\tau = \tau_{friction} + G\epsilon^2 c$
$\tau = G\epsilon^2 c$
MU-27851

Fig. 6.

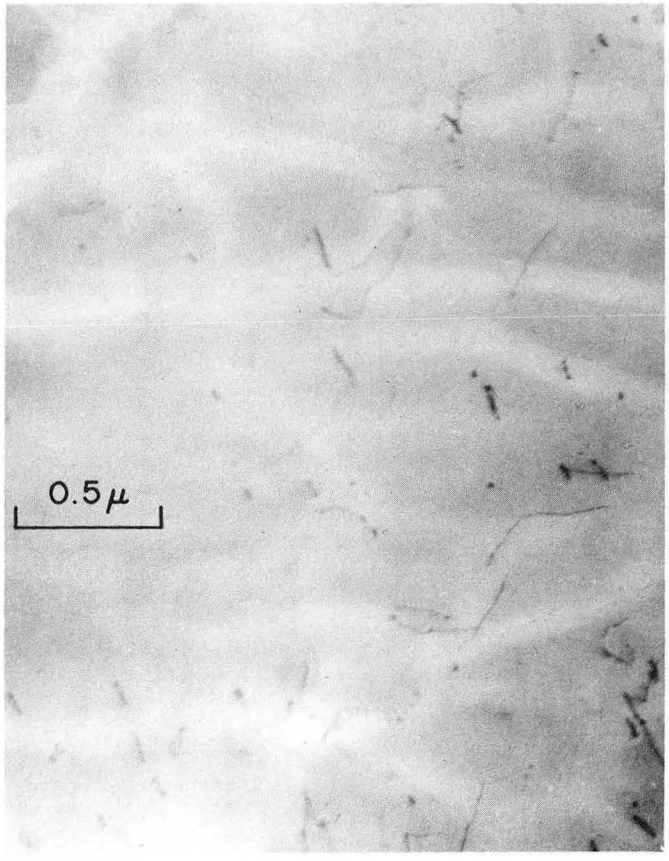

ZN-3463

Fig. 7(a).

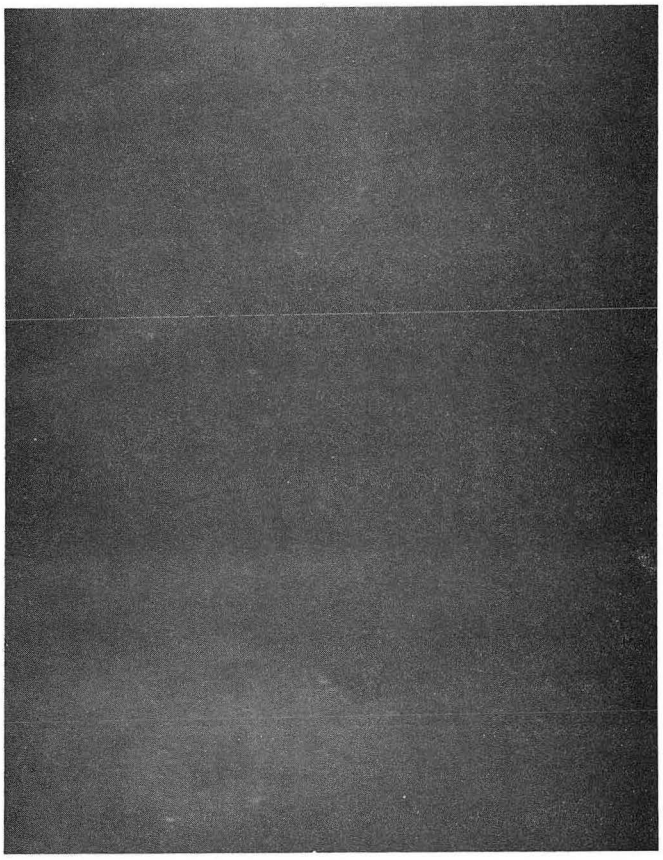

ZN-3464

Fig. 7(b).

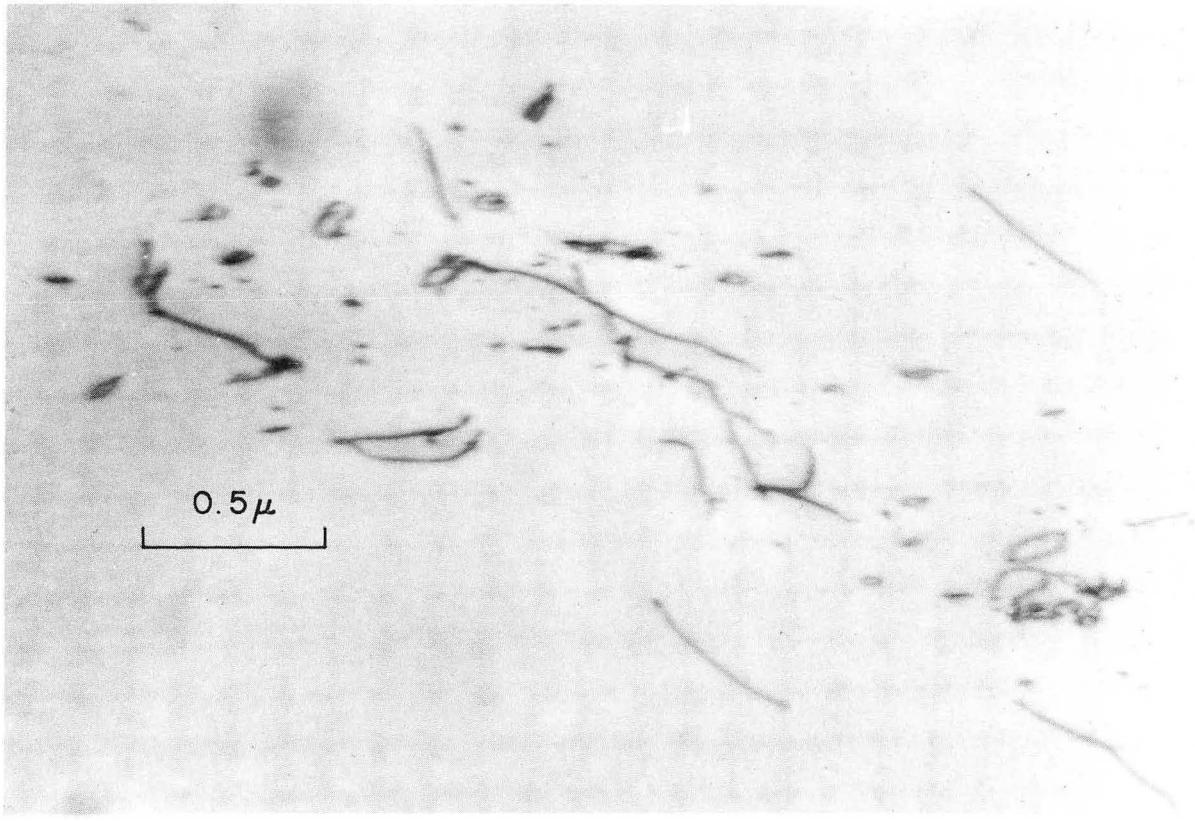

ZN-3453

Fig. 7(c).

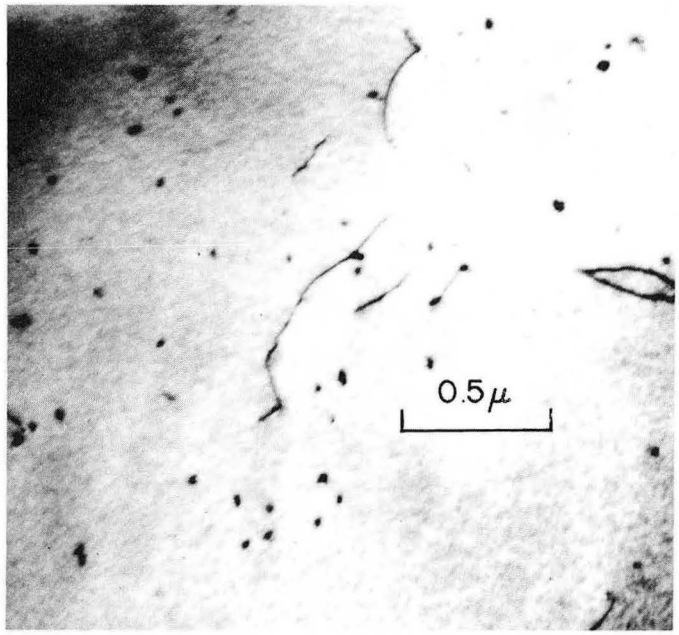

ZN-3454

Fig. 7(d).

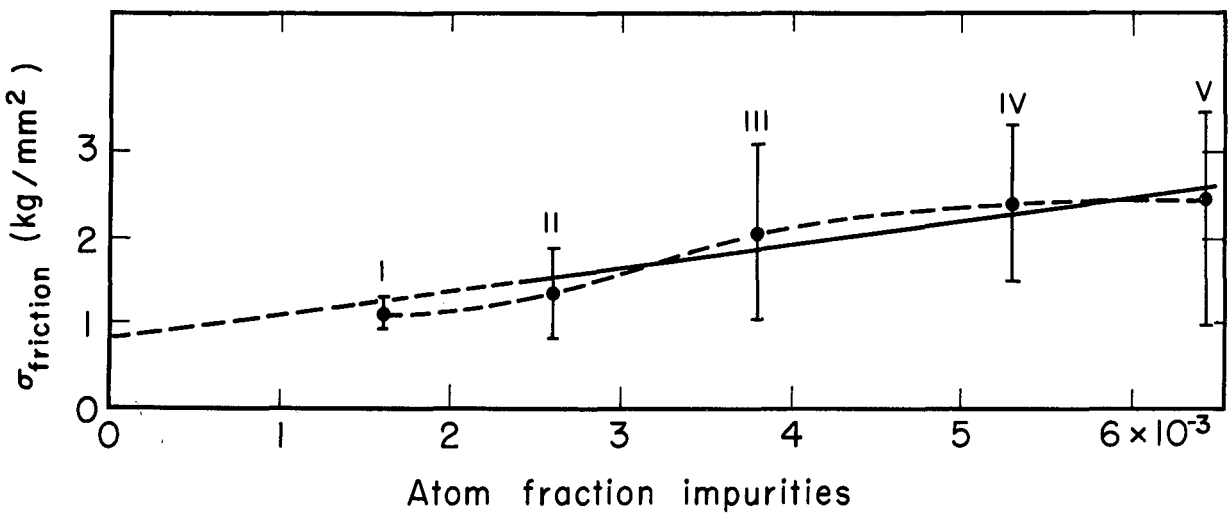

MU-29052

Fig. 8.

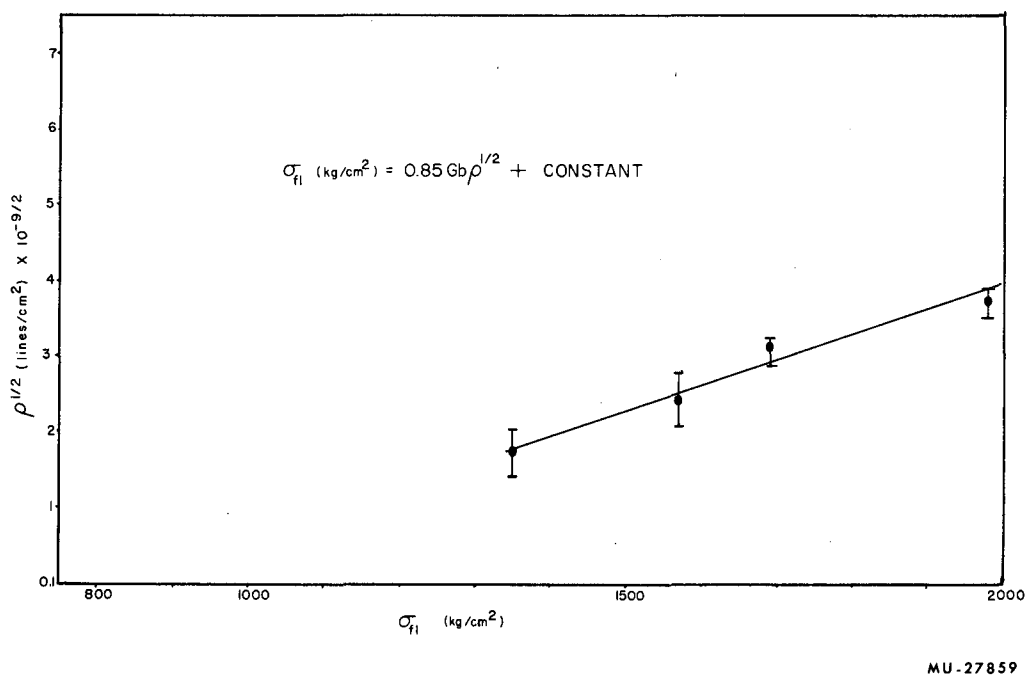
σ_{fl} (kg/cm^2) = 0.85 Gb$\rho^{1/2}$ + CONSTANT
$\rho^{1/2}$ (lines/cm^2) X 10$^{-9/2}$
0.1
1
2
3
4
5
6
7
800
1000
1500
2000
σ_{fl} (kg/cm^2)
MU-27859

Fig. 9.

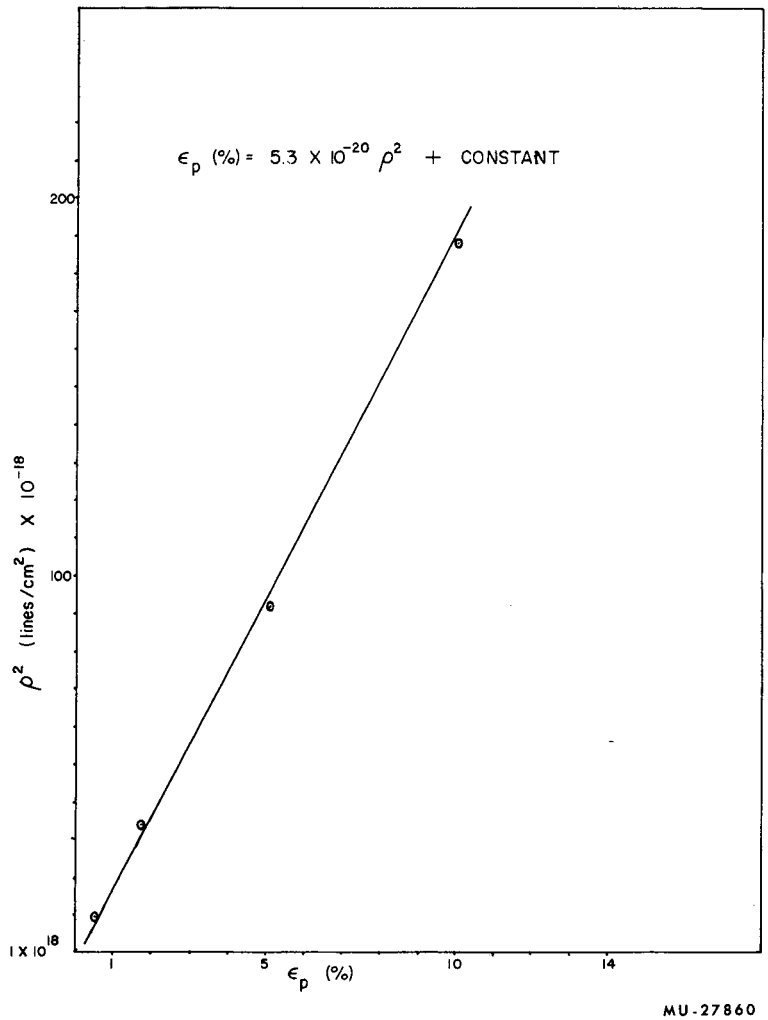
ϵ_p (%) = 5.3 X 10^{-20} ρ^2 + CONSTANT
200
100
1 X 10^{18}
ρ^2 (lines/cm^2) X 10^{-18}
1
5
10
14
ϵ_p (%)
MU-27860

Fig. 10.

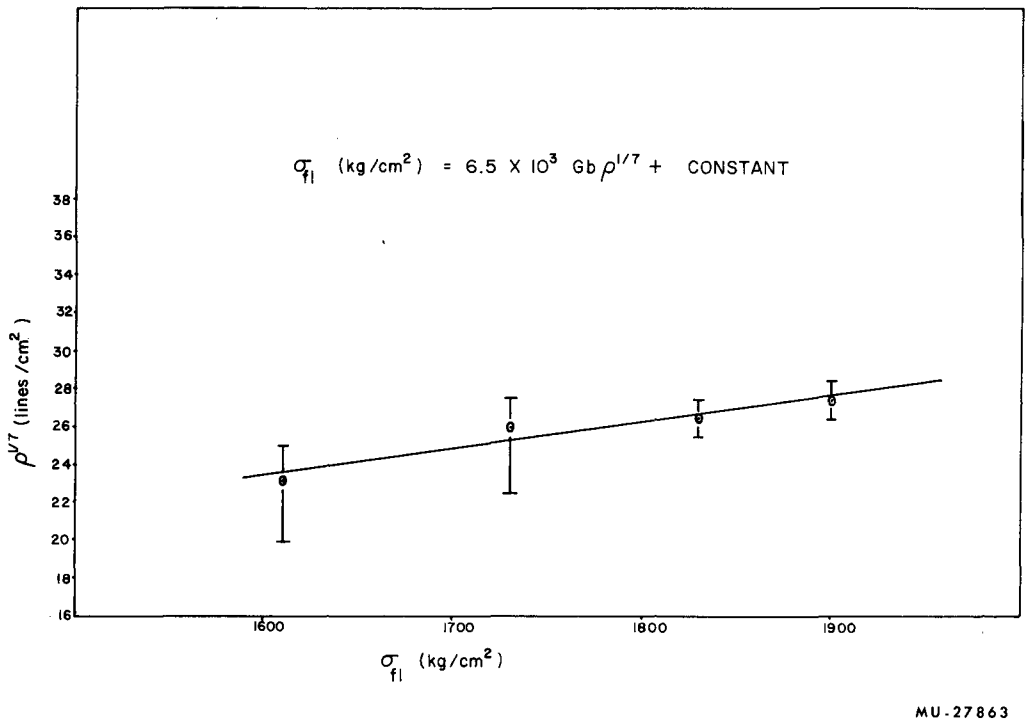
σ_{fl} (kg/cm^2) = 6.5 X 10^3 Gb $\rho^{1/7}$ + CONSTANT
$\rho^{1/7}$ (lines/cm^2)
38
36
34
32
30
28
26
24
22
20
18
16
1600
1700
1800
1900
σ_{fl} (kg/cm^2)
MU-27863

Fig. 11.

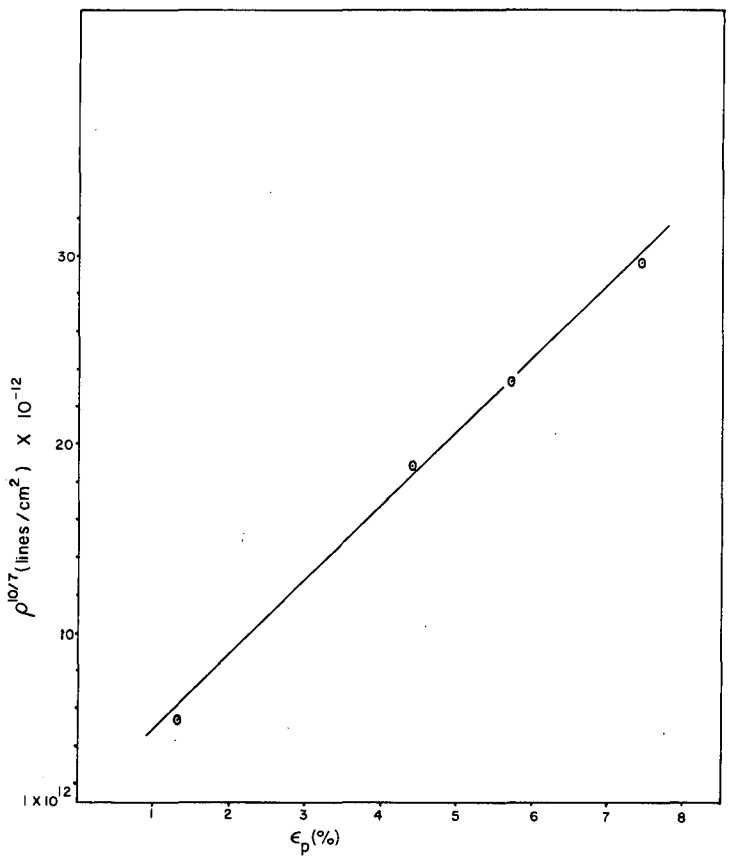

MU-27864

Fig. 12.

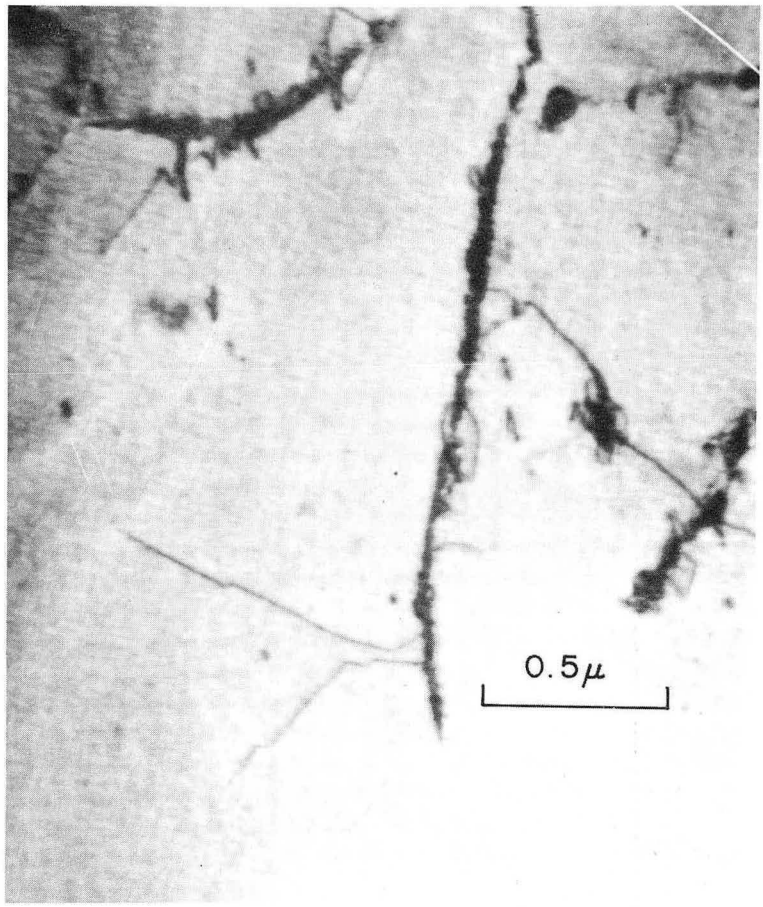

ZN-3468

Fig. 13(a).

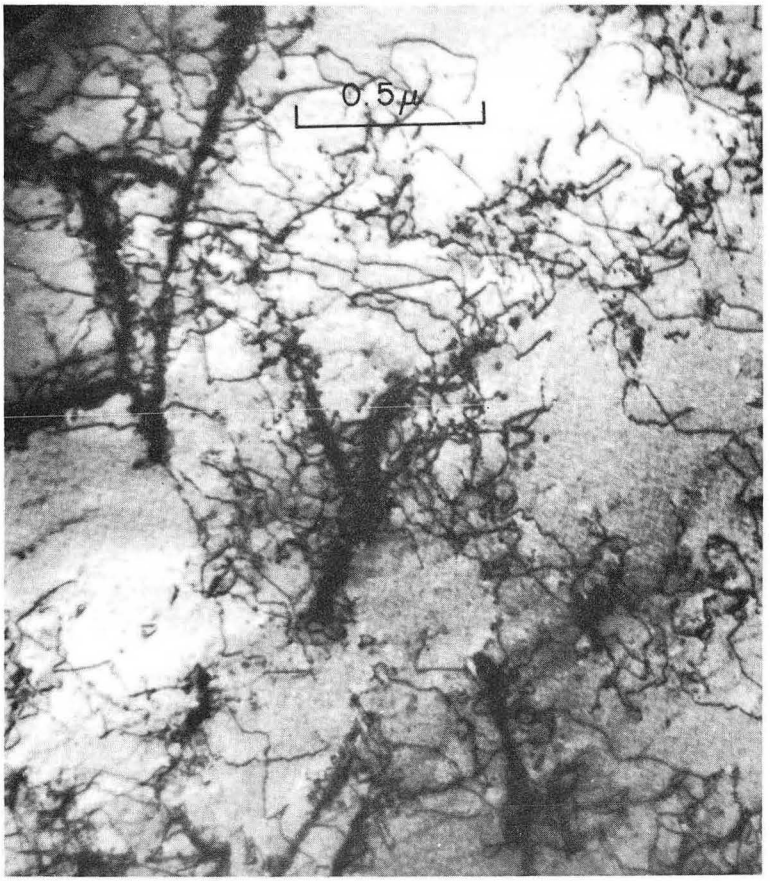

ZN-3469

Fig. 13(b).

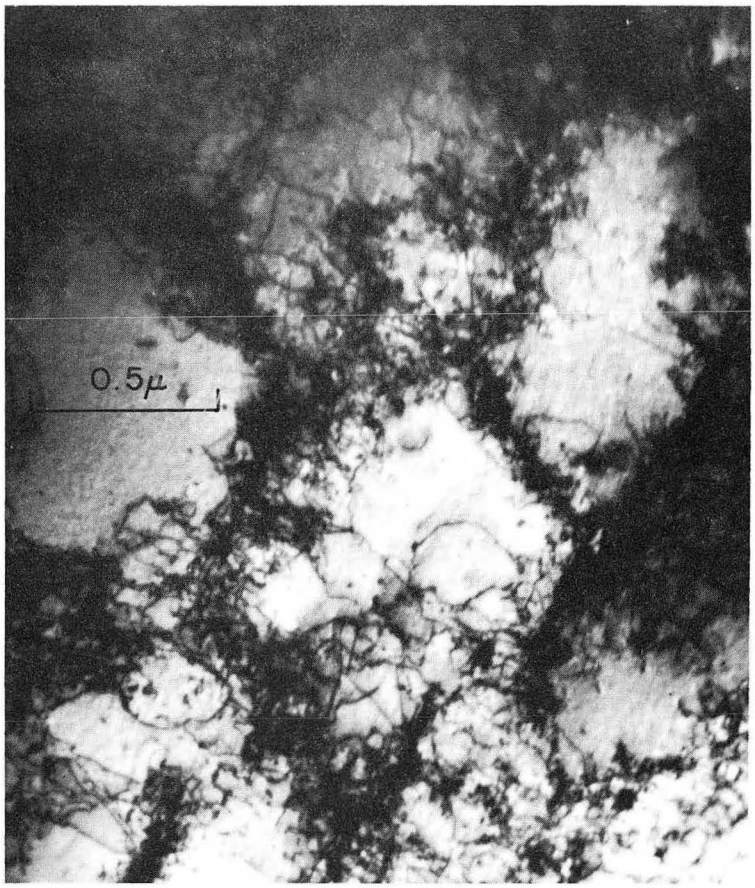

ZN-3470

Fig. 13(c).

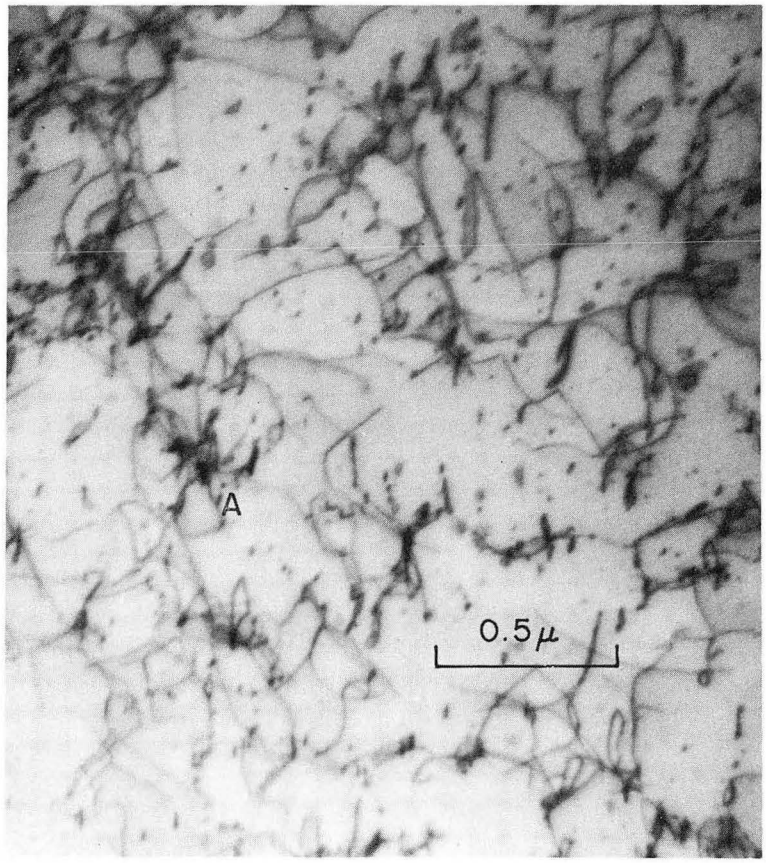

ZN-3455

Fig. 14(a).

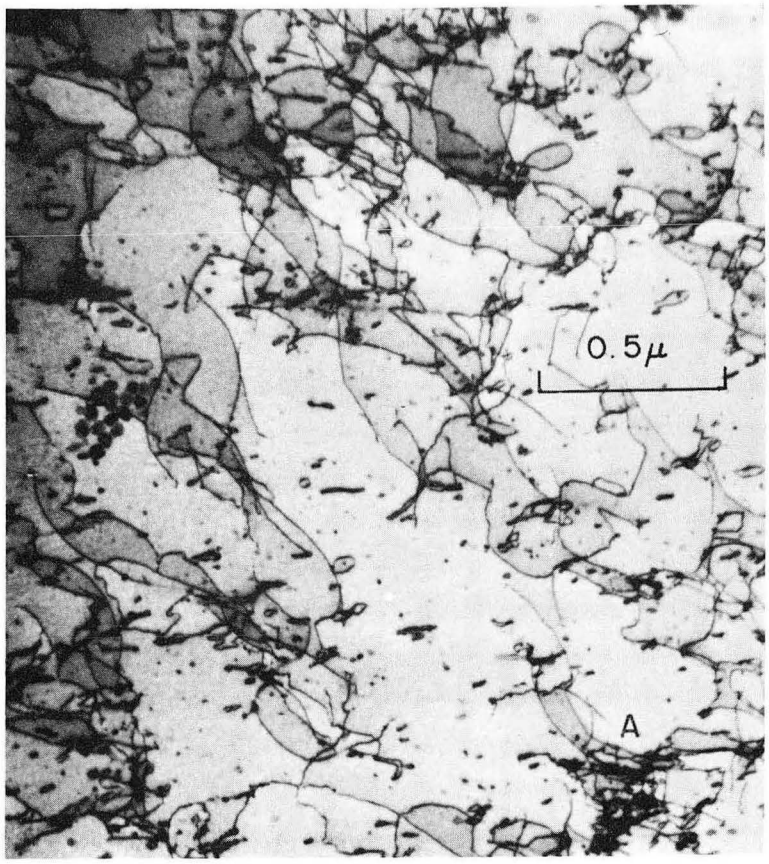

ZN-3456

Fig. 14(b).

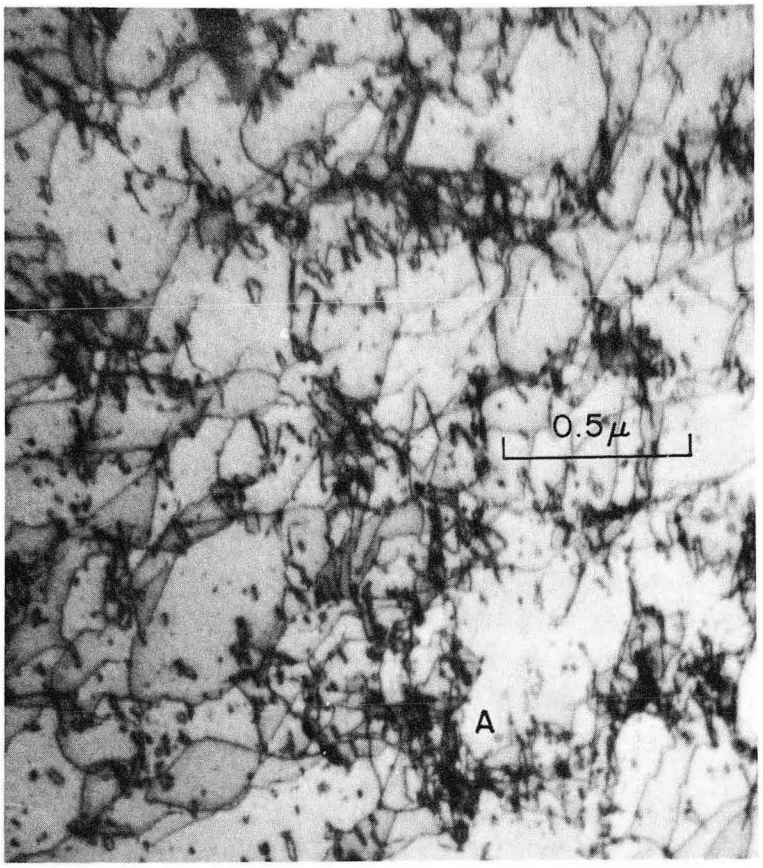

ZN-3457

Fig. 14(c).

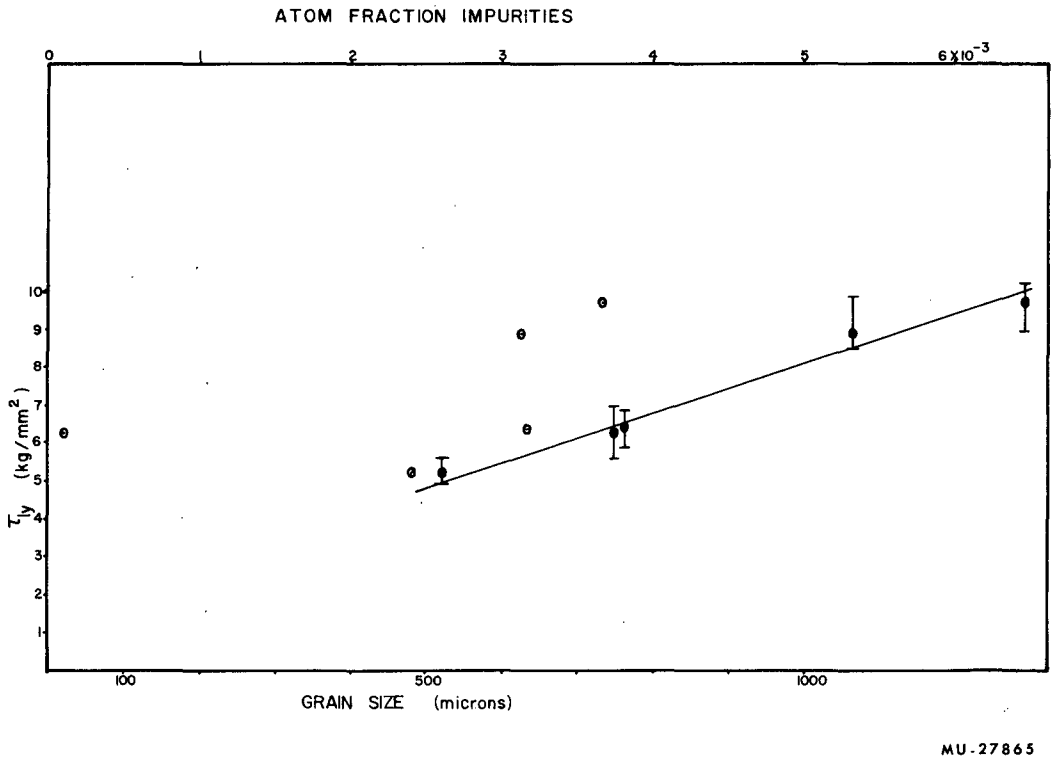
ATOM FRACTION IMPURITIES
0
1
2
3
4
5
6X10^-3
10
9
8
7
6
5
4
3
2
1
τ_ly (kg/mm²)
100
500
1000
GRAIN SIZE (microns)
MU-27865

Fig. 15.

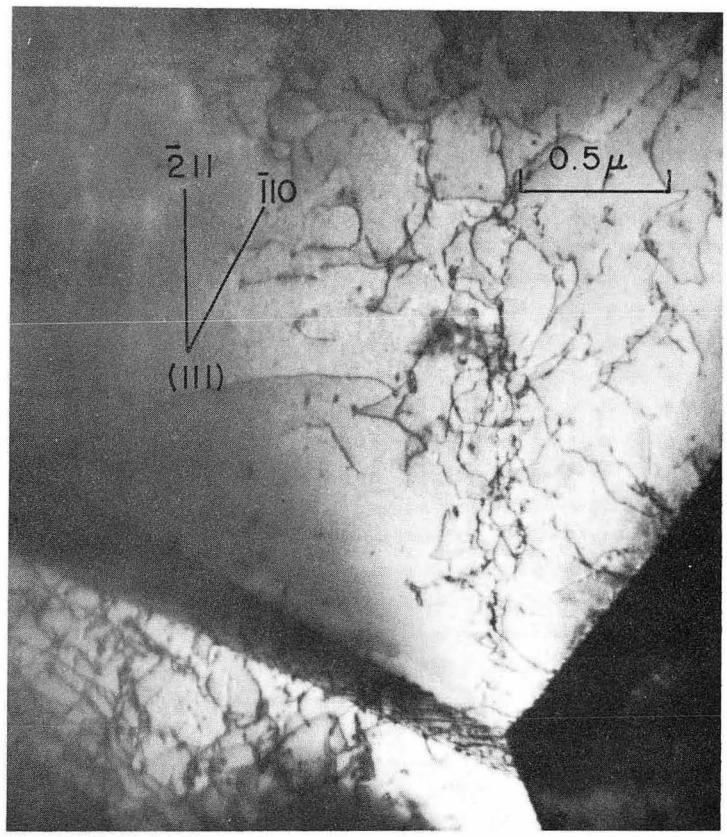

ZN-3462

Fig. 16.

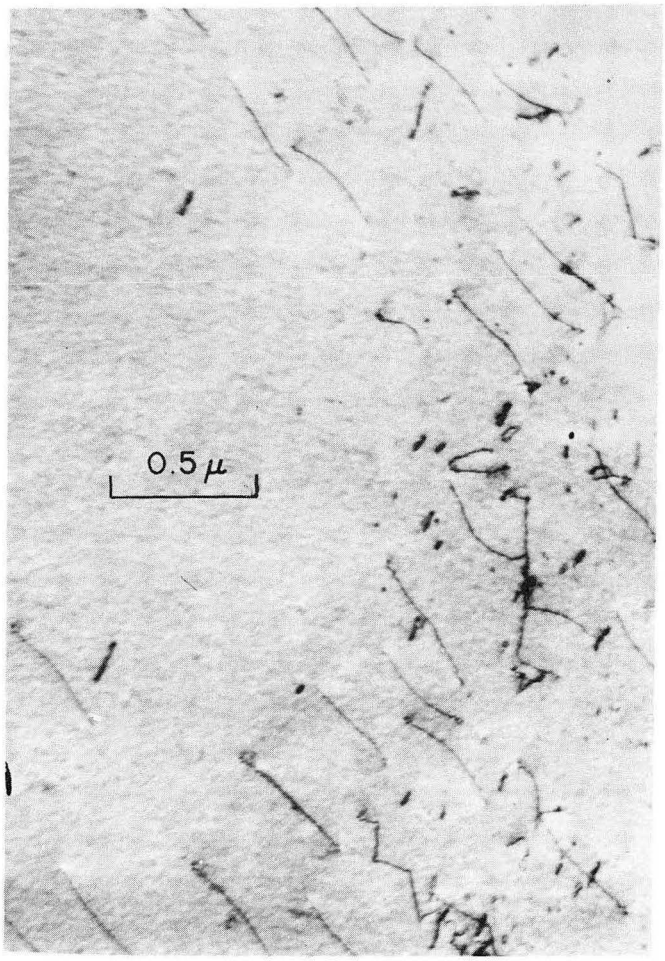

ZN-3458

Fig. 17(a).

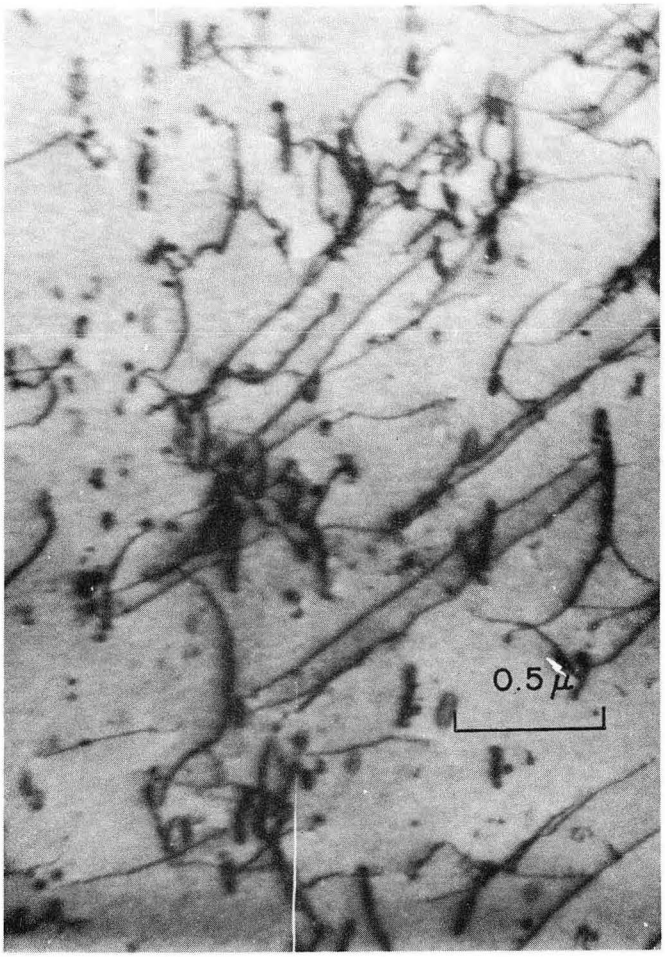

ZN-3459

Fig. 17(b).

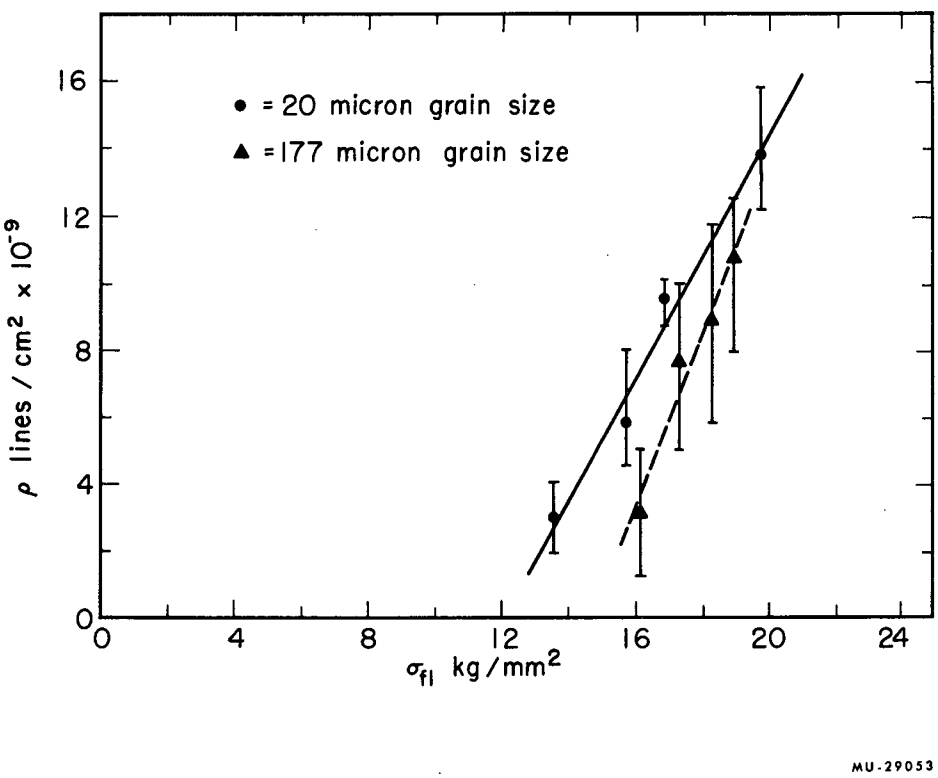
● = 20 micron grain size
▲ = 177 micron grain size
ρ lines / cm² x 10⁻⁹
σfl kg / mm²
0
4
8
12
16
20
24
MU-29053

Fig. 18.

This report was prepared as an account of Government sponsored work. Neither the United States, nor the Commission, nor any person acting on behalf of the Commission:

A. Makes any warranty or representation, expressed or implied, with respect to the accuracy, completeness, or usefulness of the information contained in this report, or that the use of any information, apparatus, method, or process disclosed in this report may not infringe privately owned rights; or

B. Assumes any liabilities with respect to the use of, or for damages resulting from the use of any information, apparatus, method, or process disclosed in this report.

As used in the above, "person acting on behalf of the Commission" includes any employee or contractor of the Commission, or employee of such contractor, to the extent that such employee or contractor of the Commission, or employee of such contractor prepares, disseminates, or provides access to, any information pursuant to his employment or contract with the Commission, or his employment with such contractor.